Slowly rocking symmetric, spatially periodic Hamiltonians: The role of escape and the emergence of giant transient directed transport

D. Hennig[1,a], L. Schimansky-Geier[1], and P. Hänggi[2,3]

[1] Institut für Physik, Humboldt-Universität Berlin, Newtonstr. 15, 12489 Berlin, Germany
[2] Institut für Physik, Universität Augsburg, Universitätsstr. 1, 86135 Augsburg, Germany
[3] Department of Physics, National University of Singapore, Singapore 117542, Republic of Singapore

Abstract The nonintegrable Hamiltonian dynamics of particles placed in a *symmetric*, spatially periodic potential and subjected to a periodically varying field is explored. Such systems can exhibit a rich diversity of unusual transport features. In particular, depending on the setting of the initial phase of the drive, the possibility of a *giant* transient directed transport in a symmetric, space-periodic potential when driven with an *adiabatically* varying field arises. Here, we study the escape scenario and corresponding mean escape times of particles from a trapping region with the subsequent generation of a transient directed flow of an ensemble of particles. It is shown that for adiabatically slow inclination modulations the unidirectional flow proceeds over giant distances. The direction of escape and, hence, of the flow is entirely governed whether the periodic force, modulating the inclination of the potential, starts out initially positive or negative. In the phase space, this transient directed flow is associated with a long-lasting motion taking place within ballistic channels contained in the non-uniform chaotic layer. We demonstrate that for adiabatic modulations all escaping particles move ballistically into the same direction, leading to a giant directed current.

1 Introduction

Transport phenomena play a fundamental role in many physical systems. In this context, dissipative ratchet dynamics has attracted considerable interest over the past years. Particles placed into periodic but sawtooth like potentials and driven by external forces or nonequilibrium noise create a directed flow even if the forces and noise vanishes in average. Thus unbiased forces induce a directed motion, a concept which was successfully applied to many different biological or mesoscopic systems. We refer here to the various overviews on molecular and Brownian motors [1–7]. This physical concept was subsequently generalized to potential landscapes possessing reflection symmetry which in addition are subjected to asymmetrical driving [8–13] and, as well, to Hamiltonian transport in absence of dissipation and enduring agitating fluctuations [14–27].

The starting point for our investigation is a system obeying reflection symmetry, both in space and time. Being interested in the particle transport features in a non-integrable situation we study the following equation of motion

$$\ddot{q} = F_0(q) + F\,\cos(\Omega t + \Theta_0) = F_0(q) + F(t)\,. \qquad (1)$$

We consider spatially periodic forces $F_0(q) = F_0(q+1)$ such as e.g. the one provided by a completely symmetric potential $U_0(q) = -\cos(2\pi q)/(2\pi)$. The time-varying ac-force in (1), $F(t)$, periodically modulates the inclination of the space-periodic potential $U_0(q)$. This set-up destroys the integrability of the system dynamics. In particular, around the corresponding separatrix in phase space a chaotic layer develops. Like in multistable potentials the motion becomes irregular and trajectories jump erratically from one potential well to another, being not always the adjacent one. Hence particles are scattered by the nonlinear forces and, obviously, the property of a directed current will typically be lost.

Remarkably, as pointed out in prior literature [15,16], in the system (1) there results an (unexpected) asymmetry of the flux of particles, emanating from one potential well, and flowing to the left and right potential wells which indicates the existence of directed transport without breaking

[a] e-mail: hennigd@physik.hu-berlin.de

the reflection symmetry in space and time in this system. One reason for the occurrence of phase-dependent directed transport is the lowering of the symmetry of the flow in phase space by the ac-field where this asymmetry vanishes only for specific values of the initial phase Θ_0 [15].

Also of interest in this context is reference [28]. Therein the authors report further on this exceptional situation and show that directed transport is sustained on fairly long time scales despite the presence of chaos. In particular it has been demonstrated that for sufficiently small forcing frequencies, $\Omega \ll 1$, the width of the arising chaotic layer diverges leading to a strong enhancement of the chaotic transport [28].

Here we complement and extend those prior studies [15,28] to the problem of escape and successively maintaining *exclusive directed motion*. More precisely, particles from a large ensemble that are initially contained in a well of the potential have to surmount the corresponding barrier. We show that adiabatically slow modulations of the potential lead to that all of the escaping particles not only leave the potential well in the same direction but subsequently enter the regime of long-lasting transients for which the transport proceeds *unidirectional* in a ballistic fashion. The direction of this arising flow over giant distances depends on the initial phase Θ_0 about which we do not average.

That trajectories contained initially in the interior of the separatrix can escape to neighboring wells of the potential is related with sweeping across the chaotic layer and crossing the separatrix. Precisely for this situation the authors in [15] demonstrated (applying ac-forces with frequencies $\Omega \sim \mathcal{O}(1)$) that the mean time-averaged velocity of a particle ensemble decays inversely proportional with time and thus tending to zero asymptotically. In contrast, we demonstrate here that for driving with a sufficiently slow ac-field the mean time-averaged velocity attains a finite value, virtually not altering on long time scales. As we shall show this is due to the fact that there occurs only a single event of separatrix crossing, namely the one guiding a particle from the inner to the outer region. Despite that afterwards the particles closely re-approach the separatrix periodically in time further crossings are avoided.

We further provide reasonings for the occurrence of the flow on the basis of the underlying phase space structure. The only assumption we have to make is that particles which are initially trapped in the interior of the separatrix are included in the arising chaotic layer around the separatrix in phase space. We will find and discuss the situation that large ensembles of particles do not only escape from the separatrix but also move in the same direction. This in turn yields a giant current.

The paper is organized as follows: In the next section we introduce the model of the particle motion in a symmetric, periodic potential, associated with the force. The inclination of this potential is being time-periodically modulated. The structure of the phase space is elucidated. In Section 3 we investigate the influence of the modulation frequency on the formation of stochastic layers in phase space. In particular, we determine the range in which the momentum variable can vary. The analysis in Section 4 concerns the chaos-induced escape of individual trajectories from the interior of the separatrix. In the subsequent Section 5 an explanation for the effect of an enormous enhancement occurring in the adiabatically driven system is given in terms of the underlying phase space dynamics. The dynamics of ensembles of particles contained initially in the interior of the separatrix and their contributions to a directed flow are addressed in Section 6.

We close with a summary of our obtained results.

2 The forced nonlinear oscillator model

The equation (1), as a driven nonlinear Hamiltonian system in one dimension, is derived from the following Hamiltonian in (dimensionless) form

$$H = \frac{p^2}{2} + U(q,t) \equiv \frac{p^2}{2} + U_0(q) + U_1(q,t)\,. \tag{2}$$

Therein p and q denote the canonically conjugate momentum and position of a particle evolving in the periodic, spatially-symmetric potential of unit period, i.e.,

$$U_0(q) = U_0(q+1) = -\cos(2\pi q)/(2\pi)\,. \tag{3}$$

An external, time-dependent forcing field

$$U_1(q,t) = -F\sin(\Omega\, t + \Theta_0)q \tag{4}$$

serves for time-periodic modulations of the inclination of the potential U_0. We underline that the system is unbiased in the sense that the force averaged over time and space vanishes, i.e.

$$\int_0^1 dq \int_0^{T=2\pi/\Omega} dt \frac{\partial U(q,t)}{\partial q} = 0\,. \tag{5}$$

For a static inclination, i.e. for $U_1(q) = -F\,q$ the system dynamics is integrable and the solutions are contained in the level set

$$H = \frac{p^2}{2} - \frac{1}{2\pi}\cos(2\pi q) - Fq \equiv E^0\,. \tag{6}$$

There exist unstable saddles at $q_s^k = 0.5 + k - \arcsin(F)/(2\pi)$ and stable centers at $q_c^k = k - \arcsin(F)/(2\pi)$ with integer values $k = 0, \pm 1, \pm 2$ .... In the non-inclined case, $F = 0$, neighboring hyperbolic points are linked via heteroclinic connections and with inclination-modulation $F \neq 0$ each hyperbolic point is linked with itself via a homoclinic connection as illustrated in Figure 1. According to the location of the saddles to the right (left) of the centers we denote the chain of homoclinic connections in the left (right) panel as right-oriented (left-oriented). For later reference, we point to the open channel arising between two neighboring separatrix loops

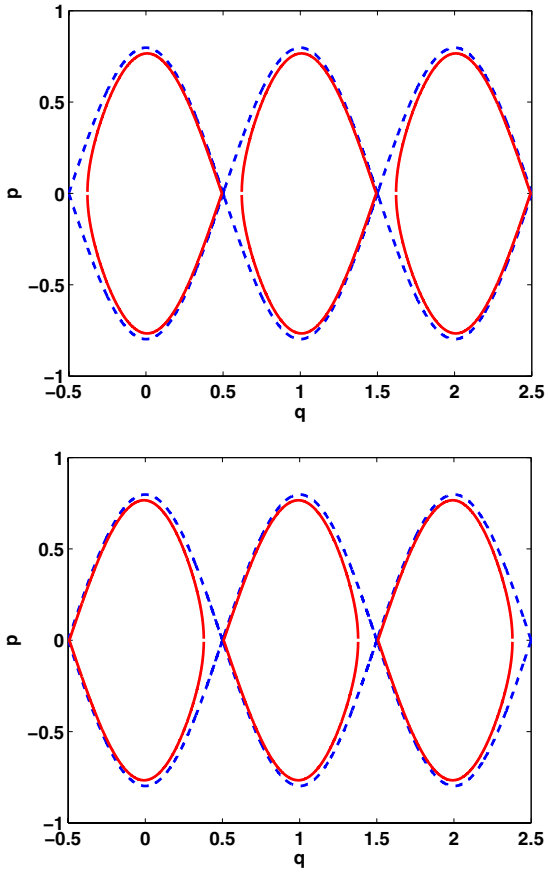

Figure 1. (Color online) The separatrix in the phase plane. Top panel: A chain of homoclinic connections (solid line) for the potential with negative inclination due to a static force of amplitude $F = 0.05$. The dashed line represents the chain of heteroclinic connections belonging to a non-inclined potential. Bottom panel: Same as in the top panel except that now the inclination is reversed, i.e. $F = -0.05$, implying a positive inclination. The visible small openings in the solid lines of the separatrix refer to the open channels for ballistic transport.

for inclined potentials. The separatrix energy attributed to the saddle at q_s^k is given by

$$E^0_{separatrix} = \frac{1}{2\pi}\left[\sqrt{1-F^2} - F[(0.5+k)2\pi - \arcsin(F)]\right]. \tag{7}$$

The maximal extension in momentum of the separatrix is

$$p^{\pm}_{max} = \pm\left(\frac{2}{\pi}\sqrt{1-F^2}\right)^{1/2}, \tag{8}$$

and the separatrix crosses the $q-$axis (turning point of the corresponding homoclinic orbit) at a value q_0 that is determined by the solution of the transcendental equation

$$E^0_{separatrix} + \frac{1}{2\pi}\cos(2\pi q_0) + F q_0 = 0\,. \tag{9}$$

Note that the separatrix loops for $F = 0$ completely comprises those for $F \neq 0$. For time-periodic modulations of the inclination which are imposed by the time-dependent potential $U_1(q,t)$, the phase space structure becomes governed by breathing of the separatrix loops where the left-oriented and right-oriented phase space structures displayed in Figure 1 represent the "turning points" of the breathing. In-between these turnings the area enclosed by a separatrix loop is periodically changing and the minimum and maximum is obtained when $\Omega t + \Theta_0 = \pi/4, 3\pi/4$ and $\Omega t + \Theta_0 = 0, \pi, 2\pi$ respectively. Moreover, with the application of a time-dependent field $U_1(q,t)$ a breaking of the integrability of the dynamics is expected. In particular, around the separatrix of the unperturbed system a chaotic layer forms. These oscillations of the separatrix between the left-oriented and right-oriented structures have to be distinguished from the pulsations of the width of the pendulum separatrix considered in [29–31]. In reference [32] the chaos dynamics in a system with periodically disappearing separatrix was considered.

3 Chaotic layers and Poincaré-plots

To illustrate the influence of the angular driving frequency on the behavior of the system we depict in Figures 2 and 3 the stroboscopic Poincaré-plots at successive periods of the driving term $T = 2\pi/\Omega$ in the $p-q-$plane for force strength $F = 0.05$, phase $\Theta_0 = 0$ and two different driving frequencies $\Omega = 0.1$ and $\Omega = 0.01$. The simulation time is chosen such that $\Omega t = 10^4$ holds and therefore, the number of periodic changes of the inclination of the potential in the simulation time interval is the same for any frequency.

The top panel in Figures 2 and 3 corresponds to stroboscopic plots at $t_k = (1/4 + k)T$ with $k = 0, 1, 2, ...$ where the potential assumes a maximal negative inclination. The bottom panel belongs to stroboscopic plots at $t_k = (3/4 + k)T$, i.e. the potential has a maximal positive inclination. For fairly fast varying modulations with $\Omega = 0.1$ a chaotic layer of small width develops around the separatrix, whereas the motion remains trapped and regular within the large island of stability with its center at the origin of the phase plane. The deformed horizontal lines above and below the large island of stability correspond to KAM tori which act as barriers for transport impeding larger upwards and downwards excursions of the momentum variable. Note that the extension of the chaotic layer in momentum direction remains equal regardless of the sign of the inclination of the potential.

Nevertheless, for slow modulation with $\Omega = 0.01$ this picture changes drastically. Many KAM tori become destroyed and the only surviving ones lie in the region of large $|p| \gtrsim 5.8$. There remains still an island of stability corresponding to bounded and regular motion inside the potential well. On the other hand, the chaotic layer has grown considerably in momentum direction compared to the previous case of $\Omega = 0.1$. Most strikingly, independent of the sign of the inclination of the potential the density of the points in the stroboscopic plots is much higher in the region of positive momentum than in the region of negative ones. Thus, the momentum variable is allowed to raise to fairly large positive values. Due to symmetry

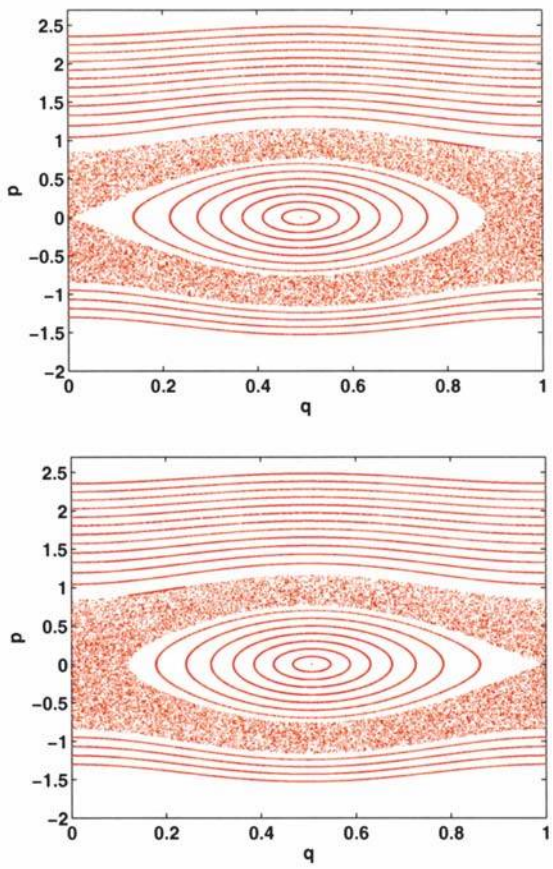

Figure 2. (Color online) Stroboscopic Poincaré-plots for an angular frequency $\Omega = 0.1$, force strength $F = 0.05$ and initial phase $\Theta_0 = 0$. The top and the bottom panel are taken at $t_k = \left(\frac{1}{4} + k\right) T$ (maximal negative inclination) and $t_k = \left(\frac{3}{4} + k\right) T$ (maximal positive inclination), respectively. The coordinate q is represented mod 1.

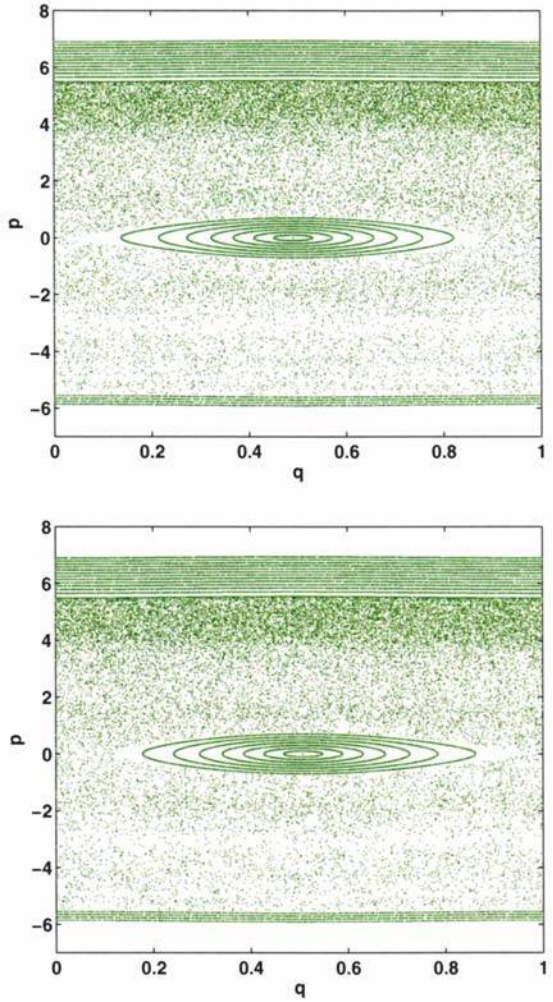

Figure 3. (Color online) Stroboscopic Poincaré-plots for an angular frequency $\Omega = 0.01$, force strength $F = 0.05$ and initial phase $\Theta_0 = 0$. The top and the bottom panel are taken at $t_k = \left(\frac{1}{4} + k\right) T$ (maximal negative inclination) and $t_k = \left(\frac{3}{4} + k\right) T$ (maximal positive inclination), respectively. The coordinate q is represented mod 1.

for an initial phase value $\Theta_0 = \pi$ of the external field, i.e. when during the first half-period $0 < t < T/2$ the inclination becomes positive, an equivalent behavior is observed except that the cloud of points now penetrates more into the range of negative p.

In the following we focus our interest on the generation of a directed flow for a large ensemble of particles where *all of them* perform *exclusively ballistic* motion in the same direction. Note that this represents a far stronger condition than merely observing directed, diffusive transport of particles as illustrated in [15]. Our set up is the following: If the potential assumes, let us say, a negative inclination due to a static force $-\partial U_1/\partial q = F$ we suppose that the dynamics of the particles is bounded in one well and the corresponding potential barrier is insurmountable, i.e. for all particles it holds that $E^0_{particle} = H_0 = p^2/2 + U_0(q) < E^0_{separatrix}$. Accordingly, the initial conditions for our simulations are distributed in the interior of the corresponding separatrix loop (see also below in Fig. 8). Obviously, with static inclination of the potential the integrable dynamics is characterized by oscillations around the stable elliptic center in the separatrix loop and hence, the particles remain trapped in the potential well. However, this scenario drastically changes when the time-dependent perturbations destroy the integrability. In particular homoclinic chaos is present in the driven dynamics. In fact, those trajectories seized by the arising chaotic layer may manage to escape from the interior region of the broken separatrix. We emphasize that this trapping-detrapping transition can only be triggered by the chaotic dynamics within the chaotic layer.

When applying the time-periodic modulation of the inclination with initial phase set at $\Theta_0 = 0$ our starting point is a non-inclined potential. Motion is then supposed to proceed towards the right. Since in the initial stage $0 < t < T/2$, the inclination passes from zero value to its maximal negative value it contributes to a continually growing positive force which promotes the desired motion towards the right. The question then is: What determines an efficient escape of trapped particles starting out

from distributed initial conditions? Is the direction of the motion of the escaped particles determined completely by the choice of the phase of the modulation term? If so, for which parameter values do the escaped particles keep moving (on average) in the preferred right direction on longer time scales?

4 Separatrix crossing and energy variations

In this section we discuss the trajectories of particles escaping from the interior of the separatrix loop. Furthermore, the possibility of energy growth after separatrix crossing for slow modulations of the inclination is studied.

Separatrix crossing and escape

In Figures 4 we depict the role of the angular frequency on the time evolution of trajectories for an initial condition contained in the region in the interior of the unperturbed separatrix in which the chaotic layer arises. For moderate and intermediate angular driving frequencies $\Omega = 1$ and $\Omega = 0.1$, respectively, the coordinate $q(t)$ behaves chaotically, exhibiting sudden and unpredictable changes of direction.

In clear contrast, for slow driving at $\Omega = 0.01$ the coordinate dynamics not only seemingly behaves more regular but also grows on average upon evolving time. Due to symmetry the direction of the motion is reversed by changing the initial position $q(0)$ to $-q(0)$ and taking for the phase $\Theta_0 = \pi$.

Furthermore, there are alternating long and short intervals during which the particle moves straightforwardly towards the right and left, respectively. Correspondingly, the momentum $p(t)$ evolves in phases with positive value (motion towards the right) that are longer lasting than the phases when the momentum is negative (leftwards motion) (see also further below in Fig. 7). As Figure 4 also reveals, the directed motion is maintained on a very long time scale where the coordinate assumes huge values. Further details concerning the time scale of unidirectional motion are contained in Section 6. In the bottom panel of Figure 4 one recognizes that for times $t \gtrsim 10^3$ the trajectory is trapped in a *ballistic channel* where the particle behaves effectively like a free particle propagating ballistically. Notice that the simulation time interval $T_s = 2 \times 10^6$ is equivalent to almost 8×10^5 and 3184 times the period duration for harmonic oscillations near the bottom of a potential well and the external modulation, respectively.

Such motion in a ballistic channel occurs for the complex dynamics of systems with a mixed phase space [33–38]. In more detail the (broad) chaotic layer is not uniform and contains cantori which can severely restrict the transport in phase space and thus effectively partition the chaotic layer bounded from below and above by non-contractible KAM tori [34–36]. Islands of regular motion that are situated at the upper and lower boundary of the layer in the vicinity of the confining KAM tori possess

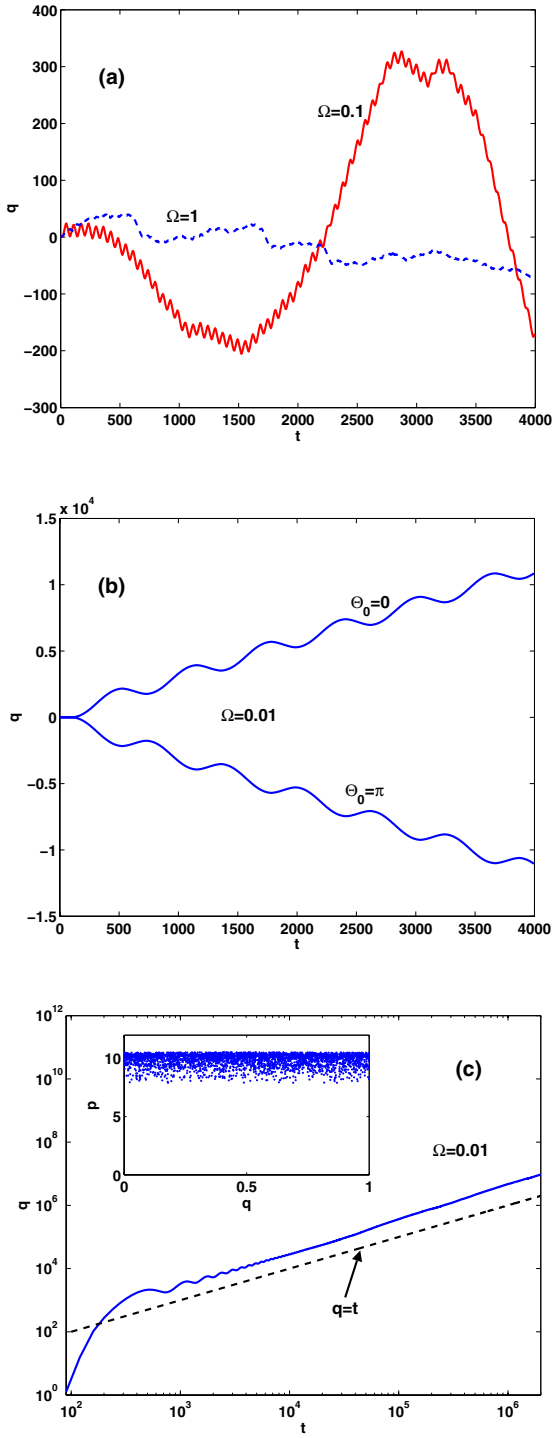

Figure 4. (Color online) Time evolution of the coordinate $q(t)$ depicted with panels (a-c) for three different angular driving frequencies Ω (indicated in the corresponding panels (a)-(c)) but equally chosen initial conditions $p(0) = 0$ and $q(0) = 0.423$. The remaining parameter values are $F = 0.05$ and $\Theta_0 = 0$. In the central panel (b) we also depict the trajectory for initial coordinate $q(0) = -0.423$ and phase $\Theta_0 = \pi$ for which the motion proceeds in the negative direction. In the bottom panel (c) the long-lasting ballistic motion of the particle is illustrated. Note the large values for the simulation times $> 10^6$ in panel (c). The inset depicts a stroboscopic Poincaré plot (at $t_k = Tk$) of the trajectory, revealing the motion in a ballistic channel.

non-zero winding numbers and thus facilitate transport. The motion around these islands is characterized by the stickiness to them [34–36], that can lead to trapping of the trajectory for a long time resulting in ballistic motion [37,38]. For some islands the sticking times to the boundary of the islands can be anomalously long [39,40].

Energy variations

It is illustrative to consider the difference,

$$\Delta E = E_{particle} - E_{separatrix} \tag{10}$$

between the particle energy

$$E_{particle} = \frac{p^2}{2} + U_0(q) - F\sin(\Theta)q\,, \tag{11}$$

and the energy of the "frozen" separatrix at time t

$$E_{separatrix} = U_0(q_s^k) - F\sin(\Theta)q_s^k\,, \tag{12}$$

where $\Theta = \Omega t + \Theta_0$ and $q_s^k = 0.5 + k + \arcsin(F\sin(\Theta))/(2\pi)$ denote the instantaneous position of the corresponding hyperbolic point when the trajectory traverses the actual range

$$\begin{aligned} q_s^{k-1} \le q \le q_s^k \qquad &\text{if} \qquad p > 0 \\ q_s^k \le q \le q_s^{k+1} \qquad &\text{if} \qquad p < 0\,. \end{aligned} \tag{13}$$

(Note that as q is a dynamical variable so is k.)

As Figure 5 reveals, for a fast modulation $\Omega = 1$ the energetic difference ΔE changes frequently the sign, corresponding to the trajectories' repeated leaving and reentering of the interior of the instantaneous separatrix. Nevertheless, in-between separatrix crossings, the particle can be trapped in a potential well for some time. Since ΔE stays close to zero the trajectory remains close to the separatrix for most of the time. Decreasing the angular driving frequency to $\Omega = 0.1$ has the effect that the number of separatrix crossings diminishes. Occasionally there appear interludes during which the trajectory escapes from the separatrix region giving rise to considerable coordinate changes q (cf. Fig. 4). However, these changes are not coordinated, so that in essence no directed motion results.

This behavior drastically differs from that occurring for a slow modulation $\Omega = 0.01$. Once the trajectory has crossed the separatrix it gathers momentum as long as the inclination remains non-positive. This goes along with an increase in the energetic difference ΔE. Afterwards, during the depreciation period, i.e. when the inclination of the potential is positive, the trajectory moves back towards the instantaneous separatrix, but never actually reenters its interior region. Notably, we followed the evolution on time scales as long as 10^7 where this behavior still holds true. In other words reversions of the direction of motion proceed in an open channel between two adjacent

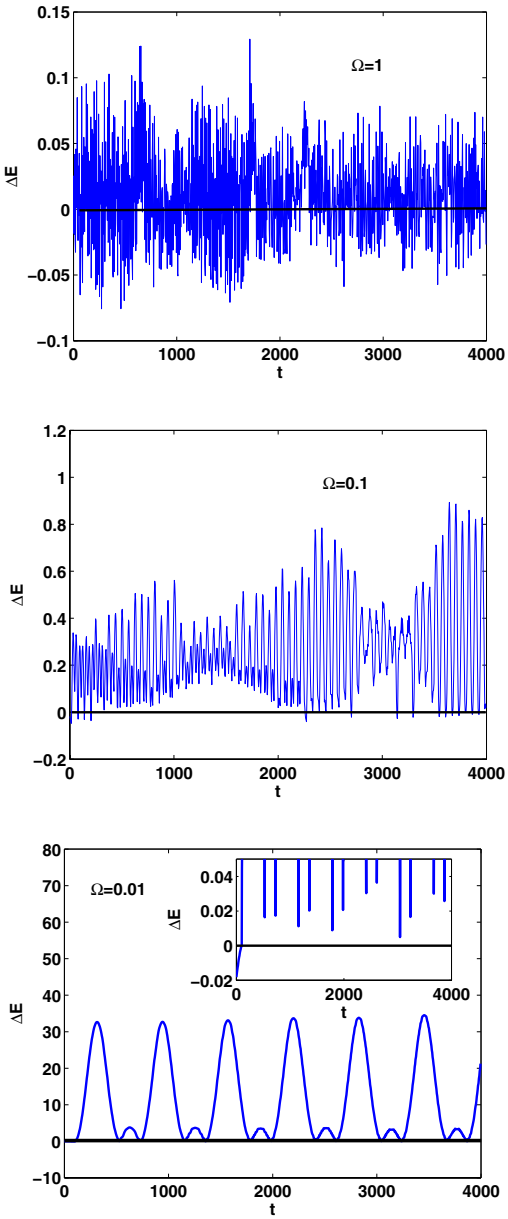

Figure 5. (Color online) Temporal behavior of the energy difference ΔE as defined in (10) for three different angular driving frequencies Ω (as indicated in the top, central and bottom panel) but equally chosen initial conditions $p(0) = 0$ and $q(0) = 0.423$. The remaining parameter values are $F = 0.05$ and $\Theta_0 = 0$. In the inset in the bottom panel one recognizes that only a single separatrix crossing takes place.

separatrix loops of the inclined potential as long as the *adiabaticity condition*

$$T_{trajectory} \ll T = \frac{2\pi}{\Omega}\,. \tag{14}$$

is satisfied, where for near-separatrix motion the period duration $T_{trajectory}$ is asymptotically determined by

$$T_{trajectory} = \frac{4}{\sqrt{2\pi}} \ln \left[\frac{4}{\sqrt{\pi |E^0_{particle} - E^0_{separatrix}|}} \right] . \tag{15}$$

For the evolution depicted in the bottom panel in Figure 4 and Figure 5 this condition (14) is obeyed.

The influence of the period of the driving force on the escape of the trajectory through the saddle point region can be elucidated as follows: Near the saddle point q_s the dynamics is given by

$$\frac{d^2q}{dt^2} + U_0''(q_s)q = F\sin(\Omega t + \Theta_0)\,, \tag{16}$$

where

$$U_0''(q_s) = \frac{d^2U_0}{dq^2}_{|_{q=q_s}} = -2\pi \equiv -a\,. \tag{17}$$

The solution of equation (16) with initial condition $p(0)$ and $q(0)$ is given by

$$\begin{aligned} p(t) = &\left[p(0) + F\cos(\Theta_0)\frac{\Omega}{a+\Omega^2} \right] \cosh(\sqrt{a}t) \\ &+\sqrt{a}\left[q(0) + F\frac{\sin(\Theta_0)}{a+\Omega^2} \right] \sinh(\sqrt{a}t) \\ &-F\frac{\Omega}{a+\Omega^2}\cos(\Omega t + \Theta_0) \end{aligned} \tag{18}$$

$$\begin{aligned} q(t) = &\frac{1}{\sqrt{a}}\left[p(0) + F\cos(\Theta_0)\frac{\Omega}{a+\Omega^2} \right] \sinh(\sqrt{a}t) \\ &+\left[q(0) + F\frac{\sin\Theta_0}{a+\Omega^2} \right] \cosh(\sqrt{a}t) \\ &-F\frac{1}{a+\Omega^2}\sin(\Omega t + \Theta_0)\,. \end{aligned} \tag{19}$$

For directed motion to occur it is important that the trajectory, after having crossed the separatrix, gathers enough momentum that a sufficient distance to the separatrix attributed to the saddle point(s) of the unstable equilibrium of the next adjacent potential well(s) is reached before the inclination of the potential is reversed. Such behavior is illustrated with Figure 6 for slow driving with $\Omega = 0.01$.

From the behavior of the solution (18), (19) with initial conditions situated close to the hyperbolic point we find that for relatively fast driving with $\Omega = 1$ the distance of the trajectory immediately grows because of the still rapidly decreasing inclination of the potential being connected with increasing momentum and coordinate of the particle. Rather soon the sign of potential inclination, and thus, the direction of the particle motion are reversed while the trajectory has not departed from the region close to the hyperbolic point. Correspondingly the trajectory, whilst being still in the neighborhood of the hyperbolic point, approaches the nearby part of the adjacent separatrix (represented by the dashed line in Fig. 6) and eventually crosses it soon after the escape. Contrarily, for slower

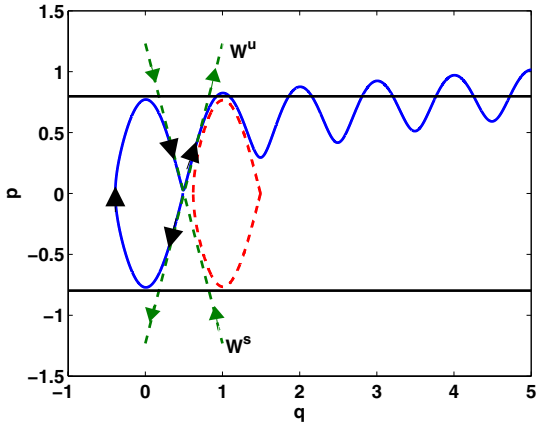

Figure 6. (Color online) Illustration of the escape from the region of the hyperbolic point in the phase plane. The particle gathers further momentum after the final libration in the interior of the separatrix has taken place (oscillatory solid line). The straight dashed lines run in the directions of the eigenvectors belonging to the eigenvalues of the system linearized about the hyperbolic point. Sufficiently close to the hyperbolic point they represent the stable and unstable manifold W^s and W^u. The two horizontal solid lines at $p_\pm = \pm\sqrt{2/\pi}$ confine the range of the momenta variations of the unperturbed separatrix. The dashed closed line to the right of the hyperbolic point represents the instantaneous separatrix loop frozen at the moment when p attains the value p_+. The parameter values are given by $F = 0.05$, $\Omega = 0.01$ and $\Theta_0 = 0$.

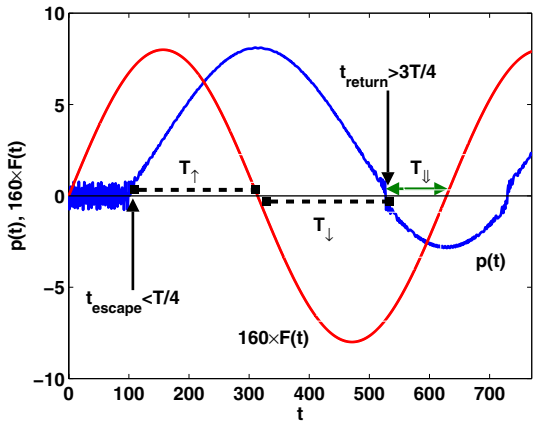

Figure 7. (Color online) Illustration of the enhanced motion at work for directed transport. Shown is the time evolution of the momentum p and the corresponding force term $F(t) = F\,\sin(\Omega t)$ with amplitude $F = 0.05$. For the sake of comparison $F(t)$ is multiplied by a factor of 160. The remaining parameter values are $\Omega = 0.01$ and $\Theta_0 = 0$. Further details are discussed in the text.

modulations $\Omega \leq 0.1$ the trajectory slowly but continually increases its distance to the nearby part of the adjacent separatrix loop. In the vicinity of the hyperbolic point the solutions (18, 19) with $\Omega \leq 0.1$ reflect this behavior.

5 Momentum growth

Here we consider the mechanism for the speed-up of a particle that has escaped from the separatrix and derive an expression for the effective gain in momentum.

Forced speed-up of particles

To gain better insight into the mechanism that causes the speed-up of the particle motion and the transition from librations to rotations we depict in Figure 7 the time evolution of the momentum for the driven dynamics together with the corresponding force $F(t) = -\partial U_1/\partial q = F\sin(\Omega\, t)$ with $\Omega = 0.01$. Up to times $t \lesssim 132$ the trajectory performs librations in the potential well. During the evolution the particle adiabatically increases its momentum so that with each turn in the potential it approaches closer the saddle point. Eventually, a separatrix crossing takes place when the trajectory is in the vicinity of the hyperbolic point where the motion becomes highly irregular, due to the intricate dynamics connected with the transversal intersections of the invariant manifolds [41,42]. Subsequently to such an escape, the motion proceeds along the direction of the unstable manifold of the hyperbolic equilibrium as further illustrated in Figure 6. Most importantly, the separatrix crossing occurs at an instant of time $t_{escape} < T/4$, for which the negative inclination has not yet reached its maximum. During the ongoing particle motion towards the right the momentum variable performs small-amplitude oscillations, while its average value grows monotonically. Eventually, the largest value $p = \sqrt{2/\pi}$ on the unperturbed separatrix (indicated by the upper straight line in Fig. 6) is exceeded. As the inclination of the potential assumes increasingly negative values the particles' momentum is raised further. At the end of the enhancement period, designated by $T_\uparrow = T/2 - t_{escape}$ in Figure 7, the momentum has grown to a maximum value of $p_{max} = 8$. Subsequently, when for $t > T/2$ the inclination of the potential is positive, the particle is in the phase of depreciation, denoted by $T_\downarrow$. Then, the momentum is reduced steadily and reverts to zero value at an instant of time $t_{return} = T/2 + T_\downarrow > 3T/4$. Due to symmetry, one obtains that $T_\uparrow = T_\downarrow$.

However, after reversal, i.e. when $p < 0$, there remains only comparatively little time, namely $T_\Downarrow = T - t_{return} < T/4$, during which the motion to the left is enhanced. Consequently, the asymmetry in the enhancement and depreciation phases, viz. the fact that $T/2 - t_{escape} > T/4 > T - t_{return}$, serves for a rather long period of rightwards motion compared to the leftwards motion. Therefore the effective motion of the particle proceeds to the right.

Momentum gain

In fact the momentum gain for a particle exerted to the force $F(t) = F\sin(\Omega t + \Theta_0)$ can be estimated as follows: Without loss of generality we consider phases in the interval $0 \le \Theta_0 \le \pi/2$ leading to large motion towards positive momenta if the particles escape at instants of time t_{escape} such that $\Omega t_{escape} + \Theta_0 \le \pi/2$ is satisfied. Then there remains the time interval $t_{escape} < t \le (\pi - \Theta_0)/\Omega$ during which the particle still experiences an enhancement in the right direction. For times $(\pi - \Theta_0)/\Omega < t \le (2\pi - \Theta_0)/\Omega$ the force acts in the opposite direction. In particular for $t_{return} \le t \le (2\pi - \Theta_0)/\Omega$ the momentum evolves with its sign reversed compared to the previous enhancement period. One obtains then

$$\begin{aligned}\Delta p &= \left(\int_{t_{escape}}^{(\pi-\Theta_0)/\Omega} + \int_{t_{return}}^{(2\pi-\Theta_0)/\Omega}\right) d\tau \dot{p} \\ &= \left(\int_{t_{escape}}^{(\pi-\Theta_0)/\Omega} + \int_{t_{return}}^{(2\pi-\Theta_0)/\Omega}\right) \\ &\quad \times d\tau\,[-\sin(2\pi q) + F\sin(\Omega\tau + \Theta_0)]\,. \end{aligned} \tag{20}$$

Due to symmetry, it holds that $t_{return} = (2\pi - \Theta_0)/\Omega - t_{escape}$. Furthermore, for small Ω the oscillating part connected with the first term in the integral averages to zero on the time scale $t_{escape} \le t \le (2\pi - \Theta_0)/\Omega$ and we find

$$\Delta p = 2\frac{F}{\Omega}\cos(\Omega\, t_{escape} + \Theta_0)\,. \tag{21}$$

In general, the smaller Ω the higher is the gain in momentum (see also [28]). In principle, for a sufficiently small frequency Ω the gain can become arbitrarily large. Δp is non-negative only if

$$t_{escape} < \frac{\frac{\pi}{2} - \Theta_0}{\Omega}\,. \tag{22}$$

Integrating over the interval of escape times with the phase Θ_0 being held fixed yields the integrated momentum gain

$$\begin{aligned}\langle \Delta p\rangle &= \int_0^{(\pi/2-\Theta_0)/\Omega} dt_{escape}\Delta p(t_{escape}) \\ &= 2\frac{F}{\Omega^2}[1 - \sin\Theta_0]\,. \end{aligned} \tag{23}$$

In conclusion, the integral momentum gain is at its maximum at $\Theta_0 = 0$ and diminishes monotonically towards zero at $\Theta_0 = \pi/2$, underlining the vital (symmetry-breaking) role of the initial phase Θ_0 for the enhancement process (see also [15]).

6 Ensemble dynamics and current

In this section we investigate the behavior of the driving induced current for an ensemble of trapped particles. Their initial conditions are distributed such that if the potential had the static inclination F the associated trapped trajectories cannot cross the corresponding separatrix loop. Likewise, as done in section 4 for the chaos-induced detrapping, we apply a time-periodic modulation of the inclination where the potential is initially non-inclined, i.e. we use a fixed initial phase $\Theta_0 = 0$. The main objective is to demonstrate that for imposed slow modulations a preferred direction of motion emerges although on average the potential landscape remains unbiased.

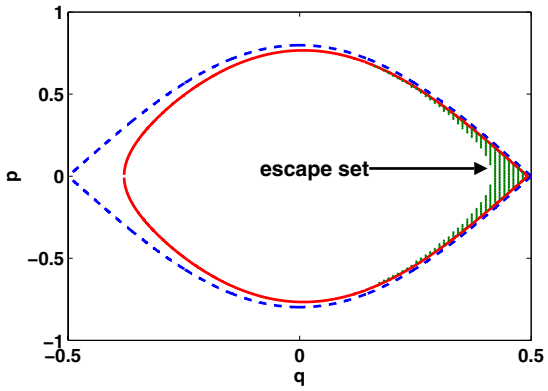

Figure 8. (Color online) The separatrix loop of the non-inclined potential (dashed line) and for the inclined potential due to a static force set at $F = 0.05$ (solid line). The escape set comprising those initial conditions that lead to escape out from the solid separatrix loop is given by the hatched area (in green online).

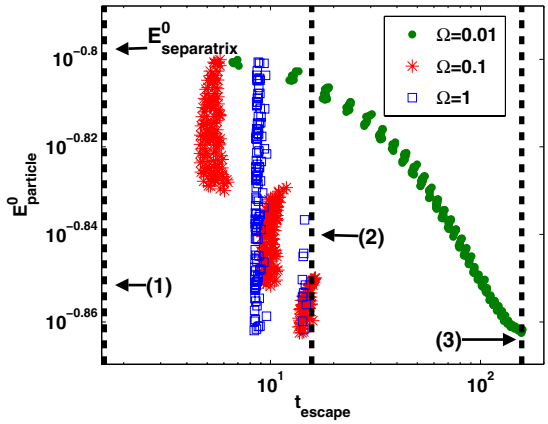

Figure 9. (Color online) The relation between the particle energy $E^0_{particle}$ and the escape time for three different frequencies as indicated in the plot. The vertical dashed lines marked as (1),(2) and (3) are at the positions of the enhancement boundary $T/4 = \pi/(2\Omega)$ for $\Omega = 1$, marked by (1), $\Omega = 0.1$, indicated as (2), and $\Omega = 0.01$, marked as (3), respectively. The remaining parameter values are $F = 0.05$ and $\Theta_0 = 0$.

6.1 Escape times

First, we identified the escape set, comprising of all those initial conditions that are contained in the interior of the static separatrix loop that lead to chaos-induced escape. To this end, the separatrix loop has been populated densely with points corresponding to initial conditions for the dynamics of the periodically driven system. The resulting escape set is displayed in Figure 8 by the hatched area. We recall that escape, i.e. the detrapping, requires a separatrix crossing. Apparently, the moment of the first separatrix crossing, i.e. the trapping-detrapping transition, governs the efficiency of the enhancement process, as discussed in Section 4. Of great importance for the speed-up of an escaped particle is that the first separatrix crossing occurs at instants of time $t_{escape} < T/4 = \pi/(2\Omega)$, which

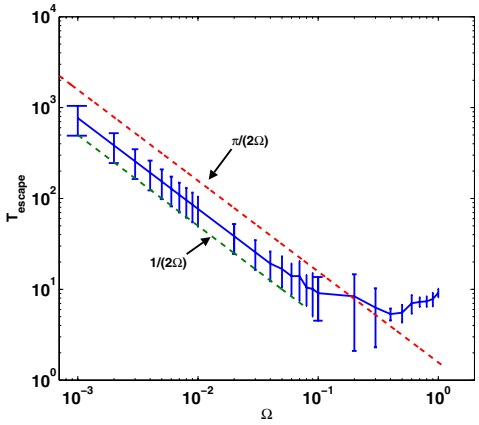

Figure 10. (Color online) The mean escape time *vs.* the angular driving frequency is plotted with error bars. The lower and upper dashed lines correspond to $T_{min} = T/4\pi = 1/(2\Omega)$ and $T/4 = \pi/(2\Omega)$, respectively. The number of particles emanating from the escape set shown in Figure 8 is taken as $N = 512$. The remaining parameter values are $F = 0.05$ and $\Theta_0 = 0$.

determines the boundary for enhancement. More specifically, according to Eq. (21), the length of the enhancement period determines the growth in momentum and thus the value of the resulting current.

From Figure 9 we deduce the corresponding time scale for escape beyond the separatrix. While for the largest angular driving frequency $\Omega = 1$ the escape takes place at times far beyond the boundary, marked as (1) in Figure 9, we note that for an intermediate angular frequency at $\Omega = 0.1$ almost all escape events occur before the corresponding enhancement boundary $T/4$, marked as (2). For slow driving at $\Omega = 0.01$, however, the scales of t_{escape} stretch over a wide range, but practically all escape events do occur at $t_{escape} < T/4$, marked as (3). Moreover, due to the irregular nature of the underlying dynamics, for an ensemble of escaping particles with distributed initial conditions the moments of their corresponding first separatrix crossing depend sensitively on the initial conditions. Trajectories starting out very close to the hyperbolic point are the first to escape, whereas for those initial conditions which are located away from the separatrix considerable time passes until escape takes place. From Figure 10, depicting the mean escape time versus the angular driving frequency Ω, we infer that for low angular frequencies $\Omega \lesssim 0.04$ the escape times are sufficiently smaller than $T/4$. In contrast, for $\Omega \gtrsim 0.04$ at least the upper error bars of the escape times are of the order of, or higher, than $T/4$. This hampers a pronounced enhancement and in turn tends to suppress the directed flow. Connecting the lower error bars of the mean escape time by a line we find that the latter is very well fitted by the expression $T_{min} = 1/(2\Omega)$. Since this line is parallel to the one of the mean escape time the latter obeys the $1/\Omega$-dependence as well.

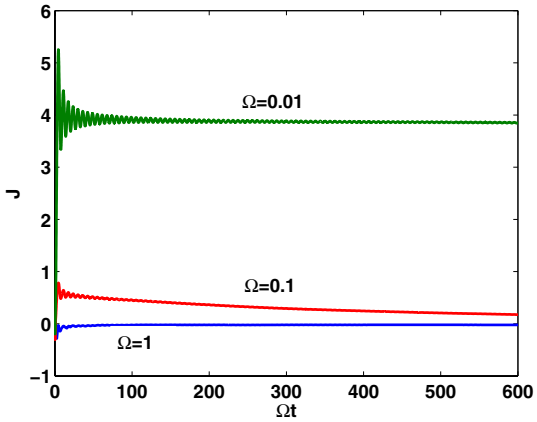

Figure 11. (Color online) Temporal behavior of the directed current defined in equation (24) for three different angular driving frequencies of the inclination-modulation force as labeled correspondingly on the graphs. The amplitude and the initial phase of the external force are set at $F = 0.05$ and $\Theta_0 = 0$, respectively. The number of particles is $N = 512$.

6.2 Averaged directed flow

With regard to directed flow we note that for $\Omega \lesssim 0.04$ we find that for the entire escape set the associated trajectories move in the *same* direction over an extended period of time. Thus, the generation of a huge, uni-directional current becomes possible. We define the directed current as the time average of the ensemble averaged momentum, i.e.,

$$J = \frac{1}{T_s} \int_0^{T_s} dt \langle p(t) \rangle \,, \tag{24}$$

with the ensemble average given by

$$\langle p(t) \rangle = \frac{1}{N} \sum_{n=1}^{N} (p_n(t) - p_n(0)) \,. \tag{25}$$

Here, N denotes the number of particles constituting the ensemble. In Figure 11 we depict the time evolution of the directed current J for moderate, intermediate and very slow modulations. The time is scaled according to $t \to \Omega t$; thus assuring that for a given simulation time T_s the number of oscillation periods of the external force is the same regardless of the value of the used angular frequency Ω. At a moderate driving frequency of $\Omega = 1$ the average flow (numerically) practically vanishes asymptotically on the displayed time scale, whereas for $\Omega = 0.1$ the decay towards zero proceeds slower. This is in compliance with the findings in [15].

In distinct contrast, however, for extreme slow driving at $\Omega = 0.01$, the mean momentum assumes a quasi-stationary regime of considerable large size. We note that our observed averaged directed current persists over a long time interval that agrees well with the explicit estimate for the duration, t_f of unidirectional motion given in [28], which adopted to our system notation reads

$$t_f \sim \frac{1}{\sqrt{2\pi}} \frac{(\sqrt{2\pi}/\Omega)^5}{\ln^4[\sqrt{2\pi}/(F\,\Omega)]} \,, \tag{26}$$

yielding for $\Omega = 10^{-2}$ and $F = 0.05$ a figure of the order of $t_f \sim 10^8$. Plotting the directed current as as a function of the angular driving frequency Ω one notices a strong decay of the current with increasing angular driving frequency (not shown here). The resulting $1/\Omega$ dependence of the current corroborates with the expression for the momentum gain given in equation (21); see also in references [15,28], providing intuitive arguments that support the strong enhancement of the chaotic transport in space.

7 Conclusion

In this work we have investigated the dissipation-less, time-dependent driven Hamiltonian dynamics of particles evolving in a symmetric, spatially periodic potential whose inclination is temporally varied periodically by an external ac-force.

We have focused interest on the generation of a directed flow of ensembles particles which are trapped in the interior of a potential well. The choice of the initial starting values is subjected to the condition that for a static inclination the trapped particles cannot escape from a potential well. Then, the only possibility left for escape from the potential well is due to the chaotic dynamics which arises in the system dynamics due to the time-dependent forcing term. In fact, upon applying the time-periodic modulation of the inclination, trajectories that become embraced by the developing chaotic layer around the broken separatrix may cross the latter. However, for fast and intermediate modulation frequency there results no substantial directed flow. This is so, because the trajectories frequently cross and re-cross the separatrix corresponding to leaving and re-entering the adjacent wells of the potential wherein the particles dwell.

For adiabatic inclination modulations we have demonstrated that for all initial conditions contained in the escape set, motion takes place in a unique direction that is controlled by the phase of the modulation term. It has been shown that the slower the modulation the larger is the gain in momentum of the escaped particles and thus the emerging asymptotic current that obeys a $1/\Omega$ dependence.

Concerning an explanation of this phenomenon it seems that the cantori, partitioning the nonuniform chaotic layer, are the less leaky the smaller the modulation frequency Ω. Research regarding the modulation frequency dependence of the sticking times to the boundary of regular islands is in progress [43]. The cantori form almost impenetrable barriers that confine trajectories for a very long but *transient* period. One should remark that eventually this transient period of directed motion terminates because the trajectory escapes through one of the holes in the cantori and accesses other regions of the chaotic layer. Therefore the motion does not necessarily

proceed unidirectionally: Unless the trajectory gets captured by ballistic channels it itinerates within the chaotic layer going along with changes of the direction of motion.

Suitable physical systems that come to mind to experimentally test our findings are periodically driven cold atom optical lattices, as recently fabricated in studying dissipative, classical ratchet dynamics [44,45]. In order to verify our multi-facetted findings of directed, dissipationless transport the use of off-resonant, far detuned laser beams is required; thus minimizing the dissipation in these cold atom set-ups: A scenario proposed in different context also for Hamiltonian quantum ratchets in references [25,46]. Moreover, the particle trapping-detrapping transitions induced by time-dependent modulations of the potential as described in this manuscript can also be applied in fluid dynamics to design particle traps in incompressible open flows as discussed in [48].

As an interesting extension of the present work we currently engage in studying this dissipation-less enhancement effect for coupled nonlinear systems which are composed of a chain of interacting particles [47].

This research was supported by SFB 555 and the VW Foundation Projects I/80425 (L.Sch.-G.) and I/80424 (P.H.). We also acknowledge very insightful and constructive discussions with S. Denisov.

References

1. P. Hänggi, R. Bartussek, Lect. Notes Phys. **476**, 294 (1996)
2. F. Jülicher, A. Ajdari, J. Prost, Rev. Mod. Phys. **69**, 1269 (1997)
3. P. Reimann, P. Hänggi, Appl. Physics A **75**, 169 (2002)
4. R.D. Astumian, P. Hänggi, Phys. Today **55**(11), 33 (2002)
5. G.N. Stratopolous, T.E. Dialynas, G.P. Tsironis, Phys. Lett. A **252**, 151 (1990); T.E. Dialynas, K. Lindenberg, G.P. Tsironis, Phys. Rev. E **56**, 3976 (1997); A. Ciudad, J.M. Sancho, G.P. Tsironis, J. Biol. Phys. **32**, 455 (2007)
6. V.S. Anishchenko, V.V. Astakhov, A.B. Neiman, T.E. Vadivasova, L. Schimansky-Geier, *Nonlinear Dynamics of Chaotic and Stochastic Systems*, 2nd edn. (Springer, Berlin-Heidelberg-New York, 2006)
7. P. Hänggi, F. Marchesoni, F. Nori, Ann. Physik (Leipzig) **14**, 51 (2005)
8. J. Luczka, R. Bartussek, P. Hänggi, Europhys. Lett. **31**, 431 (1995)
9. D.R. Chialvo, M.M. Millonas, Phys. Lett. A **209**, 26 (1995)
10. P. Hänggi, R. Bartussek, P. Talkner, J. Luczka, Europhys. Lett. **35**, 315 (1996)
11. J. Kula, T. Czernik, J. Luczka, Phys. Lett. A **214**, 14 (1996); T. Czernik, J. Kula, J. Luczka, P. Hänggi, Phys. Rev. E **55**, 4057 (1997)
12. I. Zapata, J. Luczka, F. Sols, P. Hänggi, Phys. Rev. Lett. **80**, 829 (1998)
13. S. Flach, O. Yevtushenko, Y. Zolotaryuk, Phys. Rev. Lett. **84**, 2358 (2000)
14. I. Goychuk, P. Hänggi, Lect. Notes Phys. **577**, 7 (2000)
15. O.M. Yevtushenko, S. Flach, K. Richter, Phys. Rev. E **61**, 7215 (2000)
16. I. Goychuk, P. Hänggi, J. Phys. Chem. B **105**, 6642 (2001)
17. S. Denisov, S. Flach, A.A. Ovchinnikov, O. Yevtushenko, Y. Zolotaryuk, Phys. Rev. E **66**, 041104 (2002)
18. T. Dittrich, R. Ketzmerick, M.-F. Otto, H. Schanz, Ann. Phys. (Leipzig) **9**, 1 (2000)
19. H. Schanz, M.-F. Otto, R. Ketzmerick, T. Dittrich, Phys. Rev. Lett. **87**, 070601 (2001)
20. S. Flach, S. Denisov, Acta Phys. Pol. B **35**, 1437 (2004)
21. H. Schanz, T. Dittrich, R. Ketzmerick, Phys. Rev. E **71**, 026228 (2005)
22. N.A.C. Hutchings, M.R. Isherwood, T. Jonckheere, T.S. Monteiro, Phys. Rev. E **70**, 036205 (2004)
23. S. Denisov, S. Flach, P. Hänggi, Europhys. Lett. **74**, 588 (2006)
24. T. Katsouleas, J.M. Dawson, Phys. Rev. Lett. **51**, 392 (1983)
25. J. Gong, D. Poletti, P. Hänggi, Phys. Rev. A **75**, 033602 (2007)
26. S.I. Denisov, L. Morales-Molina, S. Flach, P. Hänggi, Phys. Rev. A **75**, 063424 (2007)
27. D.V. Makarov, M.Y. Uleysky, Phys. Rev. E **75**, 065201(R) (2007)
28. S.M. Soskin, O.M. Yevtushenko, R. Mannella, Phys. Rev. Lett. **95**, 224101 (2005)
29. C.R. Menyuk, Phys. Rev A **31**, 3282 (1985)
30. J.R. Cary, D.F. Escande, J.L. Tennyson, Phys. Rev A **34**, 4256 (1986)
31. Y. Elskens, D.F. Escande, Nonlinearity **4**, 615 (1991)
32. V.T. Coppola, R.H. Rand, Nonlinear Dynamics **1**, 401 (1990)
33. G.M. Zaslavsky, *Chaos in Dynamical Systems* (Harwood, New York, 1985); *Physics of Chaos in Hamiltonian Systems* (Imperial College Press, London, 1998)
34. R.S. MacKay, J.D. Meiss, I.C. Percival, Physica D **13**, 55 (1984)
35. J.M. Greene, R.S. MacKay, J. Stark, Physica D **21**, 267 (1986)
36. J.D. Meiss, E. Ott, Physica D **20**, 387 (1986)
37. S. Denisov, S. Flach, Phys. Rev. E **64**, 056236 (2001)
38. S. Denisov, J. Klafter, M. Urbakh, S. Flach, Physica D **170**, 131 (2002); S. Denisov, J. Klafter, M. Urbakh, Phys. Rev. E **66**, 046217 (2002)
39. M.F. Shlesinger, G.M. Zaslavsky, J. Klafter, Nature (London) **363**, 31 (1993)
40. J. Klafter, G. Zumofen, Phys. Rev. E **49**, 4873 (1994)
41. S. Wiggins, *Global Bifurcations and Chaos – Analytical Methods* (Springer, New York, 1988)
42. J. Guckenheimer, P. Holmes, *Nonlinear Oscillations, Dynamical Systems, and Bifurcation of Vector Fields* (Springer, New York, 1983)
43. D. Hennig, L. Schimansky-Geier, P. Hänggi, in preparation
44. F. Renzoni, Contempory Phys. **46**, 161 (2005)
45. M. Schiavoni, L. Sanchez-Palencia, F. Renzoni, G. Grynberg, Phys. Rev. Lett. **90**, 094101 (2003)
46. S. Denisov, L. Morales-Molina, S. Flach, Europhys. Lett. **79**, 10007 (2007)
47. D. Hennig, L. Schimansky-Geier, S. Denisov, P. Hänggi, in preparation
48. I.J. Benczik, Z. Toroczkai, T. Tél, Phys. Rev. Lett. **89** 164501 (2002)